Progress in Physics of Applied Materials 1 (2021) 63–73

Semnan University

Progress in Physics of Applied Materials

journal homepage: https://ppam.semnan.ac.ir/

The effect of pulsed electron beam irradiation on surface characteristics of AM60 magnesium alloy

M. Azadi[a*], S. Rezanezhad[a], S. A. Ashraf Talesh[a], K. Ivanov[b], A. Teresov[c]

[a]*Faculty of Mechanical Engineering, Semnan University, Semnan, Iran*
[b]*Institute of Strength Physics and Materials Science of the Siberian Branch of Russian Academy of Sciences, Tomsk, Russia*
[c]*Institute of High Current Electronics of the Siberian Branch of Russian Academy of Sciences, Tomsk, Russia*

ARTICLE INFO

Article history:
Received: 5 August 2021
Revised: 28 November 2021
Accepted: 4 December 2021

Keywords:
AM60 Magnesium alloy
Process parameter
Pulsed electron beam irradiation
Surface characteristics

ABSTRACT

In this study, AM60 magnesium alloy surface modification was performed by electron beam irradiation at different energy densities of 3, 5, and 8 J/cm^2 and a pulse duration of 2-4 μs for RITM installation and 100 μs for SOLO installation. Then the surface characteristics were analyzed and the process parameters were optimized based on microscopic images with scanning electron microscopy. The element magnesium, the intermetallic phase of Al-Mn and Mg-Al ($Mg_{17}Al_{12}$) were observed on the microstructure of all samples. It is significant that due to oxidation, the MgO phase was observed in AM60 alloy which was removed by pulsed electron beam irradiation (PEBI). This technique generally caused the percentage of the AlMn phase to be lower than the raw sample and even at the energy level of 8 j/cm^2, the AlMn phase was ignored. However, the percentage of $Mg_{17}Al_{12}$ phase increased significantly after PEBI and this phase changed from block to point mode and spread throughout the material. It was found that with PEBI the surface characteristic changes and among the three levels of 33, 5, and 8 J/cm^2, 5 J/cm^2 has the lowest number of cracks and the shortest crack length.

1. Introduction

Magnesium alloys offer well-known benefits such as high specific strength, good casting capability, excellent machining, and high stiffness, and have great potential for improving vehicle fuel efficiency. For this reason, magnesium alloys are used in the automotive industry, aerospace, etc. [1,2]. They can be used in several automotive parts and engines such as ladder frames, valve covers, cylinder heads, and blocks [3-5]. However, magnesium alloys available in the market have worse mechanical properties compared to aluminum alloys [6]. One of the main problems is the low corrosion resistance of magnesium alloys, which can be improved by surface modification, which is the primary goal of this work.

Metal surface correction techniques using pulsed concentrated energy fluxes have been extensively developed in recent decades. Rapid heating, melting, and evaporation of the surface layer to which energy is given result from an energy flux concentrated on a substance. Due to the dynamic stresses created by superfast solidification in the melt zone, this material undergoes severe deformation after completing the energy pulse.

When these processes are used together, metastable states can be created in the surface layers of materials, giving them better physicochemical properties and strength, which is not possible with traditional surface treatment methods. One of these techniques is Pulsed electron beam irradiation (PEBI) [7]. Due to its efficiency, effectiveness, simplicity, and reliability, PEBI treatment is known as a superior surface correction approach compared to pulsed laser beam and ion beam techniques [8-10], some metal materials have also been observed that take benefits from its favorable effects on mechanical properties and corrosion resistance [8–13].

To improve corrosion resistance, Zhang et al. [14] used a high current pulsed electron beam (HCPEB) to modify the surface of AISI 304L austenitic stainless steel. They found that increasing the electron beam (EB) pulses reduced the corrosion of the pitting at the surface immersed in seawater. Kim et al [10] have looked at the correction of the surface of molded steel materials by the large pulsed electron beam. Kim et al. [10] have looked at the surface modification of mold steel materials by the large pulsed electron beam (LPEB). The surface quality and glossiness of KP1, KP4 significantly enhanced when the energy density increased to 10 J/cm^2. Based on the polarization test in NaCl, the surface modification reduced the corrosion rate of KP4. Rotshtein et al. [15] reviewed the results of surface-modified aluminum alloys by HCPEB. HCPEB

* Corresponding author. Tel.: +98-910-210-7280
E-mail address: m_azadi@semnan.ac.ir

DOI: 10.22075/PPAM.2021.24156.1012

irradiation improves the electrochemical impedance of Al6061 alloy. They believed the improvement was due to Al_2O_3 that forms after the irradiation and also, the second-phase particles that develop during pulsed melting.

Walker et al [16] showed corrosion for Ti-6Al-4V surfaces modified by LPEB irradiation on Ti alloys. According to OCP measurements and annular polarization curves in 3.5 wt% NaCl solution, the corrosion rate decreased from 923.2 to 5.478 nm/y. By twinning and slips, a homogeneous martensitic surface layer was created at the previous grain boundaries by 15-25 LPEB pulses on the material. Similarly, Kim et al. [12] claimed that LPBE could improve Ti-6Al-7Nb's overall surface characteristics. The corrosion impedance in 10 J/cm^2 of the energy density utilized specimens rose from 170 to 260 kΩ·cm^2 based on the findings of EIS measurements in a 1 wt.% NaCl solution. HCPEB (3 J/cm^2) can improve the surface of AZ31, according to Bo et al. [17]. In the Mg-Al binary allotropic system, the EB process selectively evaporated Mg.

Hao and Li [18] published an article in which they used HCPEB to increase the microhardness of AZ91 magnesium alloy. According to the study, the polarization corrosion current in NaCl was halved. The Al content of HCPEB-treated surfaces (about 8 μm thin-film) increased from about 9wt% to more than 30wt%, according to EDS data. Then, using XRD data, magnesium was evaporated on the main grain structure by electron beam heating. Zhang et al [19] Improved hardness as well as corrosion resistance by PEB on pure Ti, due to microstructure refinement and improved inactivation on the material surface. When commercial AZ91 magnesium alloy is treated with PEB, Gao et al. [8] found that surface formation of Al-supersaturated solid solution improves wear and corrosion resistance.

Based on the literature review, different irradiation techniques were performed on different light alloys to improve the surface properties. Such a technique is still rare in AM60 magnesium alloys and optimization of process parameters has not yet been reported for PEBI. Therefore, in this study, as a novelty, the effect of three energy density levels (3, 5, and 8 j/cm^2) on the PEBI technique on the surface properties of AM60 magnesium alloy has been investigated.

2. Materials and Experiments

The pulsed electron beam irradiation (PEBI) technique was used to change the surface characteristics of AM60 magnesium alloy. The parameters and their values in this process could be seen in Table 1. It should be noted that the surface energy (E_s) is generally in the interval of 2-15 J/cm^2, the accelerating voltage (U) is between 15 and 30 kV and the number of pulses (N) could be 1 to 40, for the RITM installation. For the SOLO installation, the pulse duration (t) could be 50 to 200 μs and the surface energy (E_s) could be considered as 3-60 J/cm^2.

For such an investigation, scanning electron microscopy (SEM) was utilized plus the energy-dispersive X-ray spectroscopy (EDS) for analyzing the chemical element. Moreover, X-ray diffraction (XRD) was also used for determining the phase in the microstructure. This study was also performed for the as-received material.

The modified surface of the material by the PEBI would have a layer depth of 1-2 μm. Therefore, the micro-hardness could not be used. Both installations for the PEBI could be seen in Fig. 1..

Fig. 1. The installation for the PEBI including (a) the RITM-I3 for with short pulse duration and (b) the SOLO with a long pulse duration

Table 1

The parameters and their values of the PEBI technique

No.	Parameter	Dimension	Value	Device	Investigation
1	Surface energy (E_s)	J/cm^2	3-5-8	RITM Installation	XRD/SEM/EDS
2	Pulse duration (t)	µs	2-4	RITM Installation	XRD/SEM/EDS
3	Pulse number (N)	-	10	RITM Installation	XRD/SEM/EDS
4	Surface energy (E_s)	J/cm^2	3*-5-8	SOLO Installation	XRD
5	Pulse duration (t)	µs	100	SOLO Installation	XRD
6	Pulse number (N)	-	10	SOLO Installation	XRD

3. Results

3.1. XRD results

Figure 2 shows the XRD pattern for the as-received materials and AM60 surface modification with surface energies of 3, 5, and 8 J/cm^2 by RITM installation energy. Figure 3 indicates such a result for the SOLO installation. As it could be seen, besides the Mg element, the intermetallic phase of Al-Mn and Mg-Al ($Mg_{17}Al_{12}$) was observed on the microstructure of all samples. These results could be confirmed by the literature [20, 21].

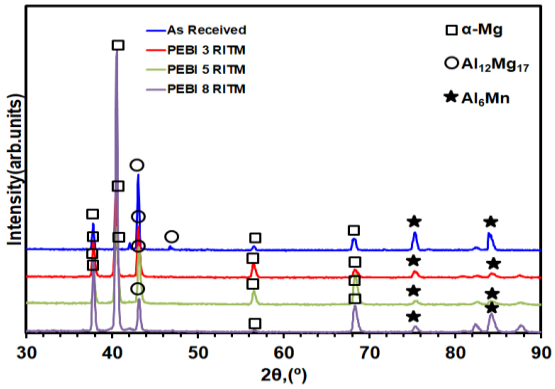

Fig. 2. The XRD pattern for the as-received material and the surface modification by the RITM installation under the surface energy of 3, 5, and 8 J/cm^2

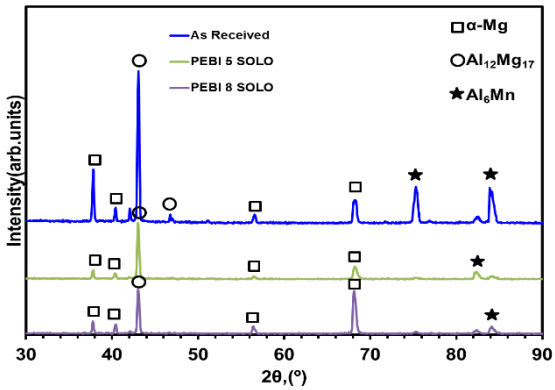

Fig. 3. The XRD pattern for the as-received material and the surface modification by the SOLO installation under the surface energy of 5 and 8 J/cm^2

3.2. EDS/SEM results

SEM images with EDS results can be seen in Fig. 4 for samples received and surface modified samples by PEBI. As can be seen in the XRD pattern of the as-received materials, the three phases include Mg (α phase), $Mg_{17}Al_{12}$ (β phase), and AlMn. In addition, the MgO phase is also seen in the microstructure according to Table 2 and Fig. 4. That is, surface oxidation has occurred.

The EDS element analysis of the surface-modified specimen by the PEBI (E_s=3 J/cm^2) is shown in Fig. 5 and Table 3 with the atomic percent and the weight percent. Moreover, obtained results of other surface energies could be observed in Fig. 6 and Table 4 (E_s=5 J/cm^2) and also, in Fig. 7 and Table 5 (E_s=8 J/cm^2).

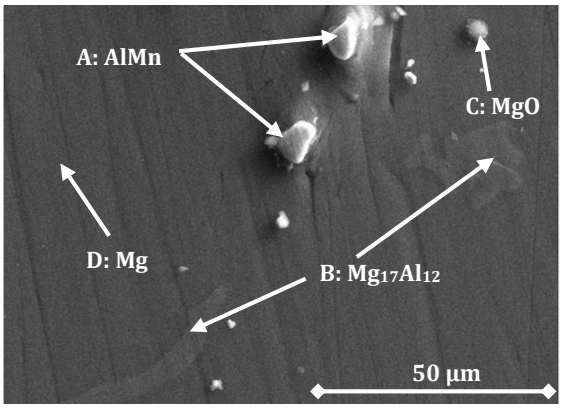

Fig. 4. The SEM image of the as-received sample

Table 2
The EDS result for the elemental analysis in the as-received sample

Point	Element	Weight percent (%)	Atomic percent (%)
Figure 4 (A)	Mg	1.65	2.58
	Al	38.75	54.76
	Si	1.95	2.65
	Mn	57.65	40.01
Figure 4 (B)	Mg	62.24	64.84
	Al	37.24	34.95
	Cu	0.52	0.21
Figure 4 (C)	Mg	68.88	60.86
	Al	2.92	2.33
	Ca	0.47	0.25
	Ni	0.68	0.25
	O	27.05	36.32
Figure 4 (D)	Mg	96.09	96.47
	Al	3.91	3.53

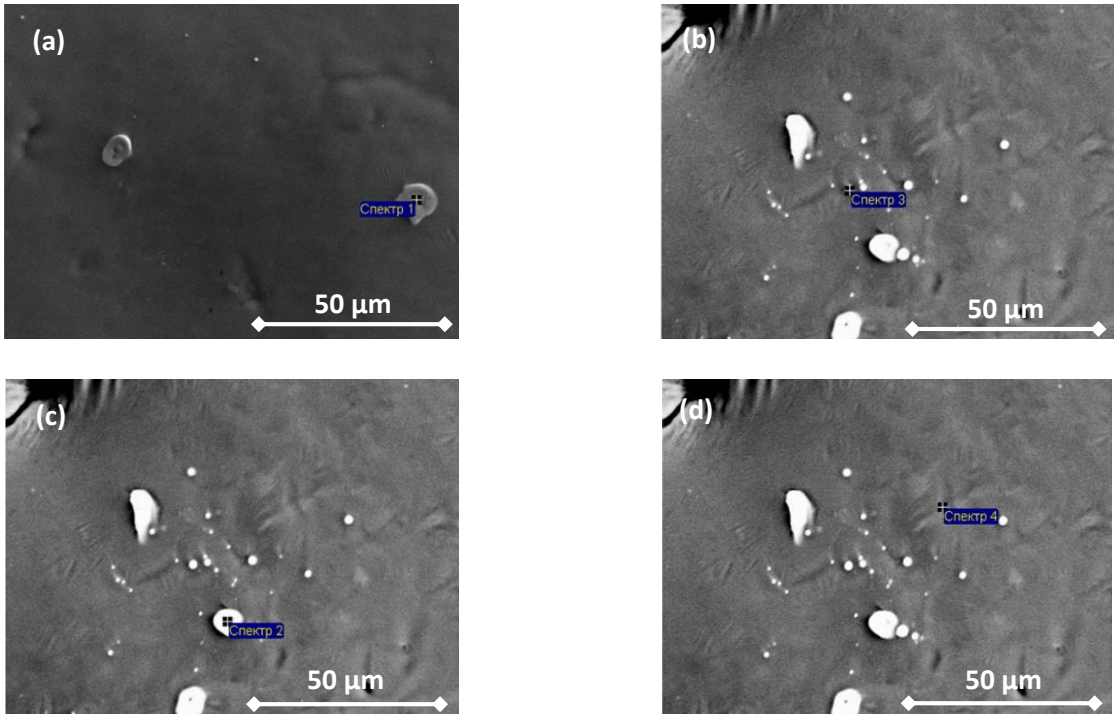

Fig. 5. The SEM image from the surface-modified AM60 alloy by the PEBI at E_s=3 J/cm^2

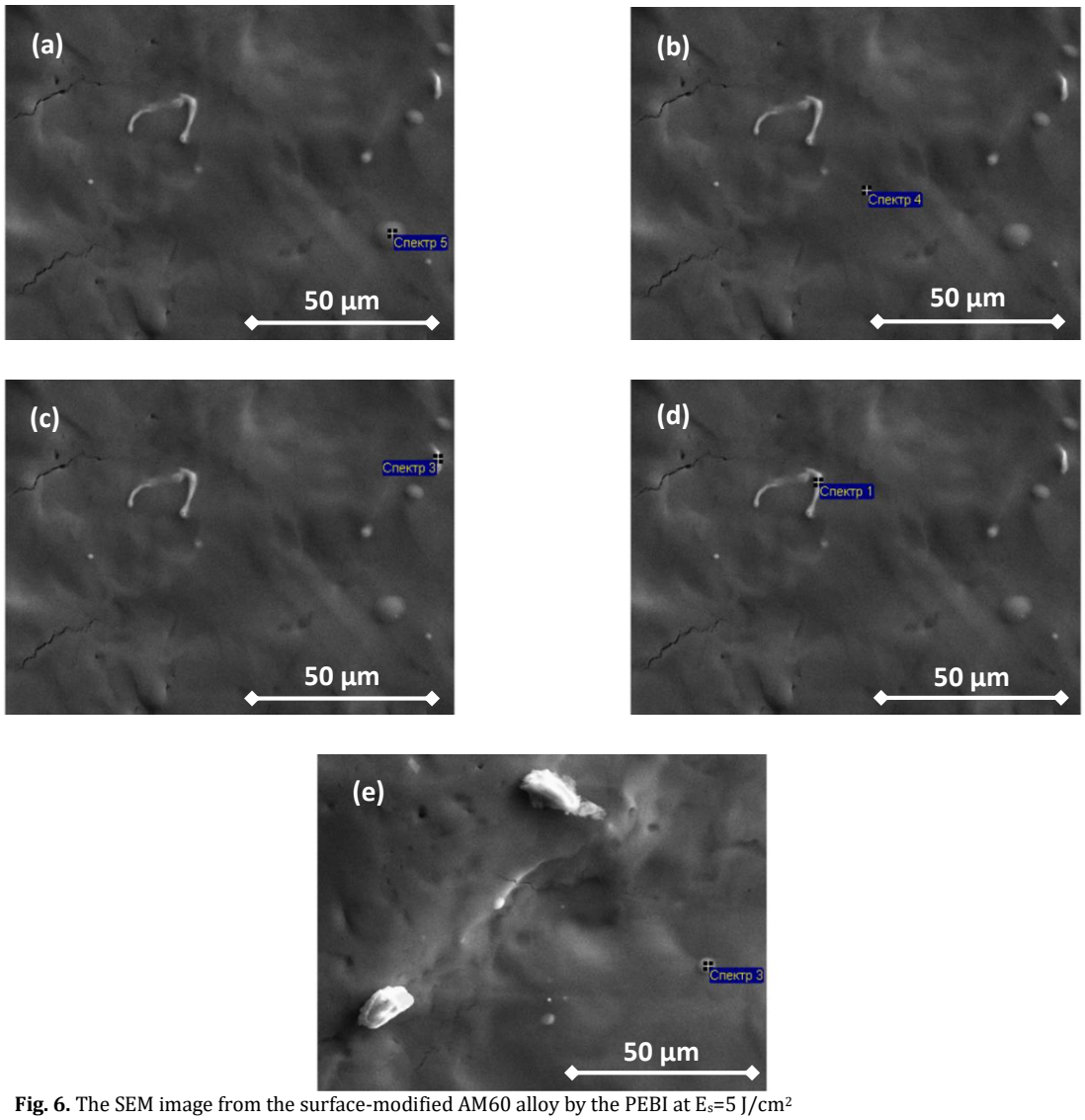

Fig. 6. The SEM image from the surface-modified AM60 alloy by the PEBI at E_s=5 J/cm^2

Table 3
The EDS results from the surface-modified AM60 alloy by the PEBI at E_s=3 J/cm^2

Point	Element	Weight percent (%)	Atomic percent (%)
Figure 5(a)	O	20.03	35.14
	Mg	8.77	10.13
	Al	33.59	34.95
	Si	1.17	1.17
	Mn	35.01	17.89
	Fe	1.44	0.72
Figure 5(b)	Mg	49.22	59.51
	Al	23.41	25.50
	Si	0.68	0.71
	Mn	26.69	14.28
Figure 5(c)	Mg	4.34	6.95
	Al	32.78	47.27
	Si	1.84	2.55
	Mn	64.04	43.23
Figure 5(d)	Mg	93.50	94.11
	Al	6.50	5.89

Table 4
The EDS results from the surface-modified AM60 alloy by the PEBI at E_s=5 J/cm^2

Point	Element	Weight percent (%)	Atomic percent (%)
Figure 6(a)	O	1.74	2.69
	Mg	72.01	73.36
	Al	25.93	23.80
	Mn	0.32	0.14
Figure 6(b)	Mg	91.60	92.71
	Al	7.59	6.93
	Mn	0.81	0.36
Figure 6(c)	Mg	35.33	45.54
	Al	28.64	33.26
	Si	1.22	1.36
	Mn	34.20	19.51
Figure 6(d)	Mg	33.84	45.44
	Al	23.58	28.53
	Si	1.28	1.49
	Mn	40.36	23.98
Figure 6(e)	Mg	82.77	84.20
	Al	17.23	15.80

Table 5
The EDS results from the surface-modified AM60 alloy by the PEBI at E_s=8 J/cm^2

Point	Element	Weight percent (%)	Atomic percent (%)
Figure 7(a)	Mg	79.13	80.91
	Al	20.59	18.97
	Mn	0.28	0.13
Figure 7(b)	Mg	83.61	84.99
	Al	16.39	15.01
	Mg	83.02	84.46
Figure 7(c)	Al	16.27	14.91
	Si	0.72	0.63
Figure 7(d)	Mg	83.24	84.79
	Al	16.40	15.05
	Mn	0.36	0.16
Figure 7(e)	Mg	16.27	24.14
	Al	29.42	39.34
	Si	1.40	1.79
	Mn	50.54	33.19
Figure 7(f)	Fe	2.38	1.53
	Mg	92.67	93.36
	Al	6.95	6.31
	Si	0.38	0.33
Figure 7(g)	Mg	73.09	75.32
	Al	26.25	24.38
	Mn	0.66	0.30
Figure 7(h)	Mg	80.66	82.23
	Al	19.34	17.77
Figure 7(i)	Mg	83.98	85.33
	Al	16.02	14.67
Figure 7(j)	Mg	83.72	85.09
	Al	16.28	14.91
Figure 7(k)	Mg	83.13	84.68
	Al	16.51	15.16
	Mn	0.36	0.16
Figure 7(l)	Mg	91.88	92.63
	Al	8.12	7.37

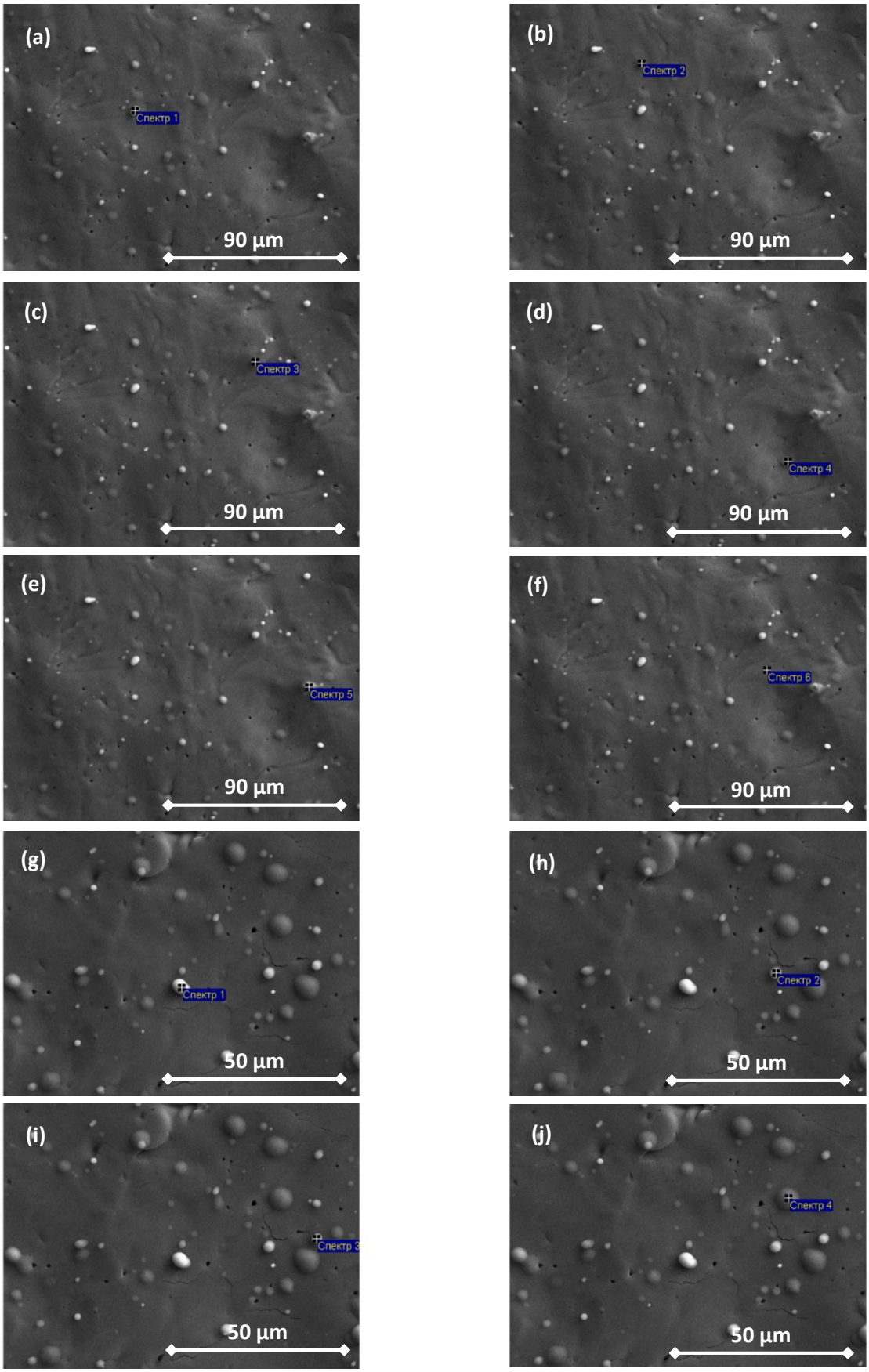
(a)
Спектр 1
90 µm
(b)
Спектр 2
90 µm
(c)
Спектр 3
90 µm
(d)
Спектр 4
90 µm
(e)
Спектр 5
90 µm
(f)
Спектр 6
90 µm
(g)
Спектр 1
50 µm
(h)
Спектр 2
50 µm
(i)
Спектр 3
50 µm
(j)
Спектр 4
50 µm

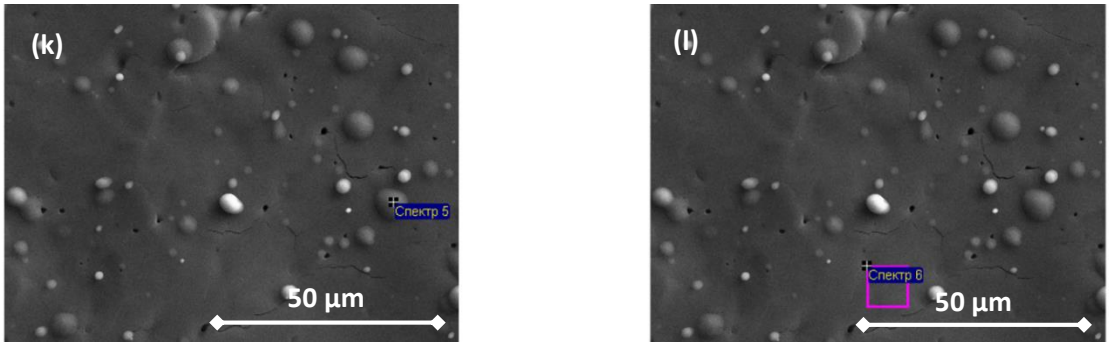

Fig. 7. The SEM image from the surface-modified AM60 alloy by the PEBI at E_s=8 J/cm^2

Figure 8 shows the SEM image of the material under study at 100X magnification. For other higher magnifications, Figu. 9 to 11 can be used.

The average number and length of cracks of the studied materials based on SEM images in different PEBI conditions are presented in Table 6.

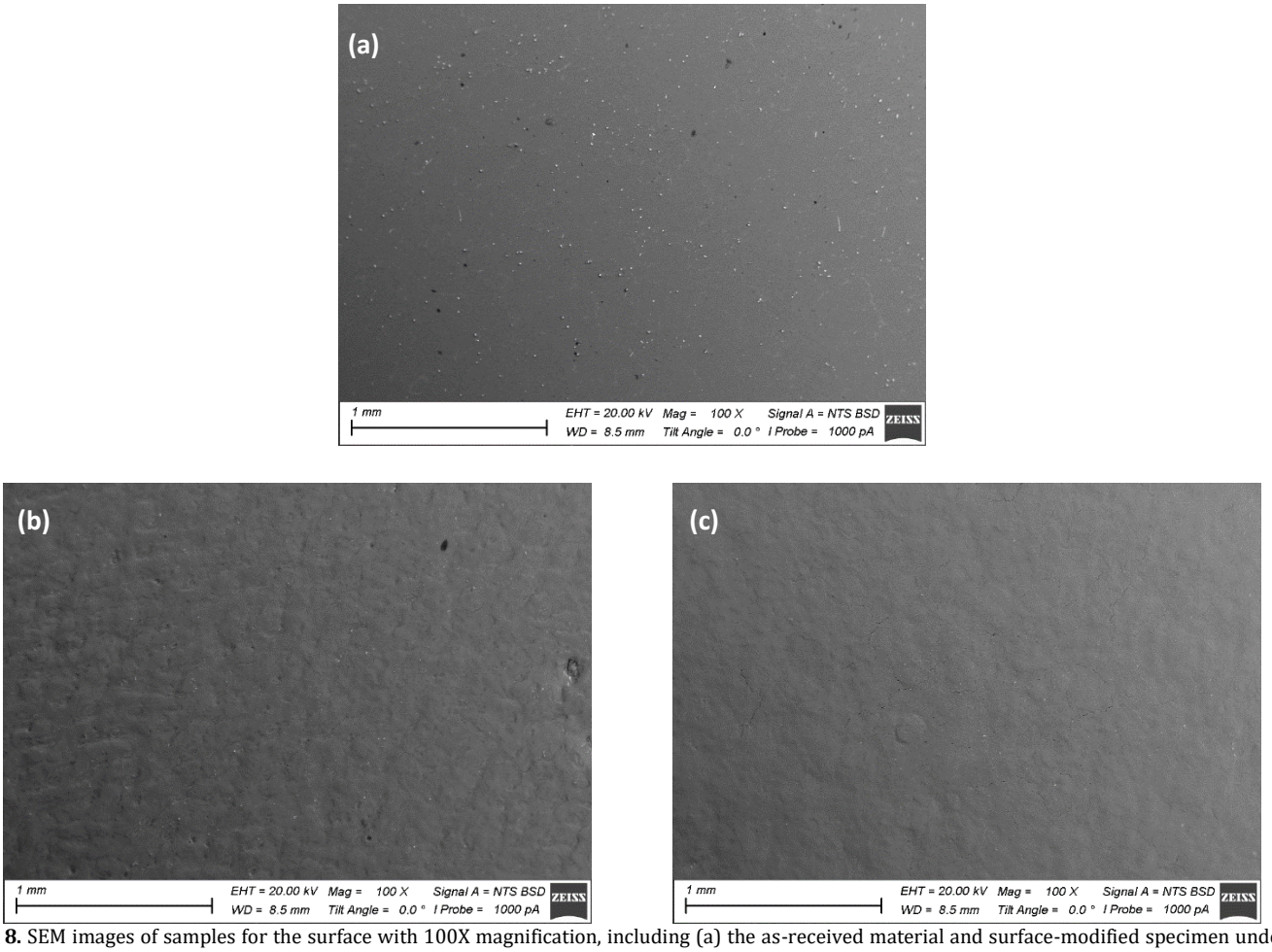

Fig. 8. SEM images of samples for the surface with 100X magnification, including (a) the as-received material and surface-modified specimen under the surface energy of (b) 5 and (c) 8 J/cm^2

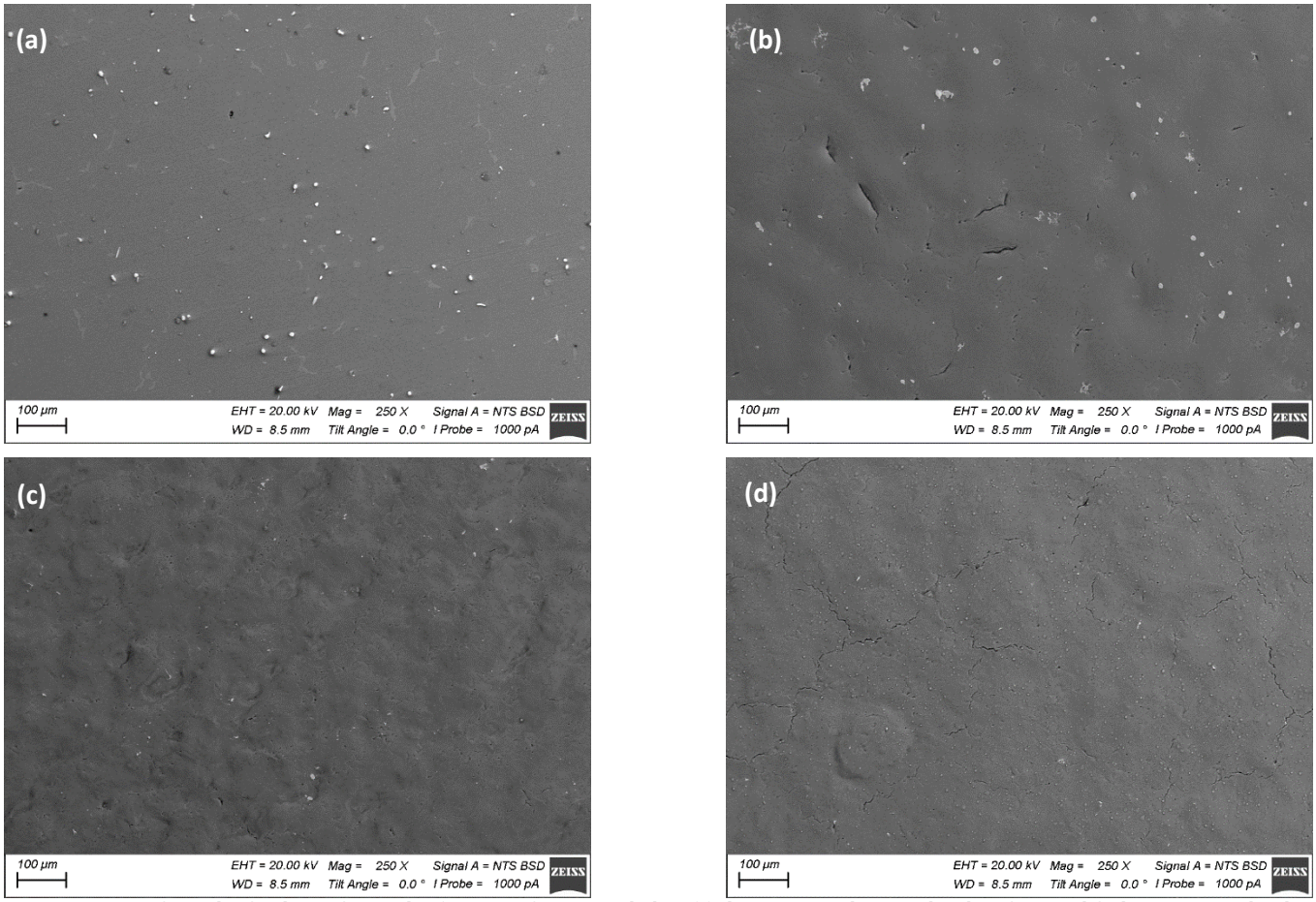

Fig. 9. SEM images of samples for the surface with 250X magnification, including (a) the as-received material and surface-modified specimen under the surface energy of (b) 3, (c) 5, and (d) 8 J/cm^2

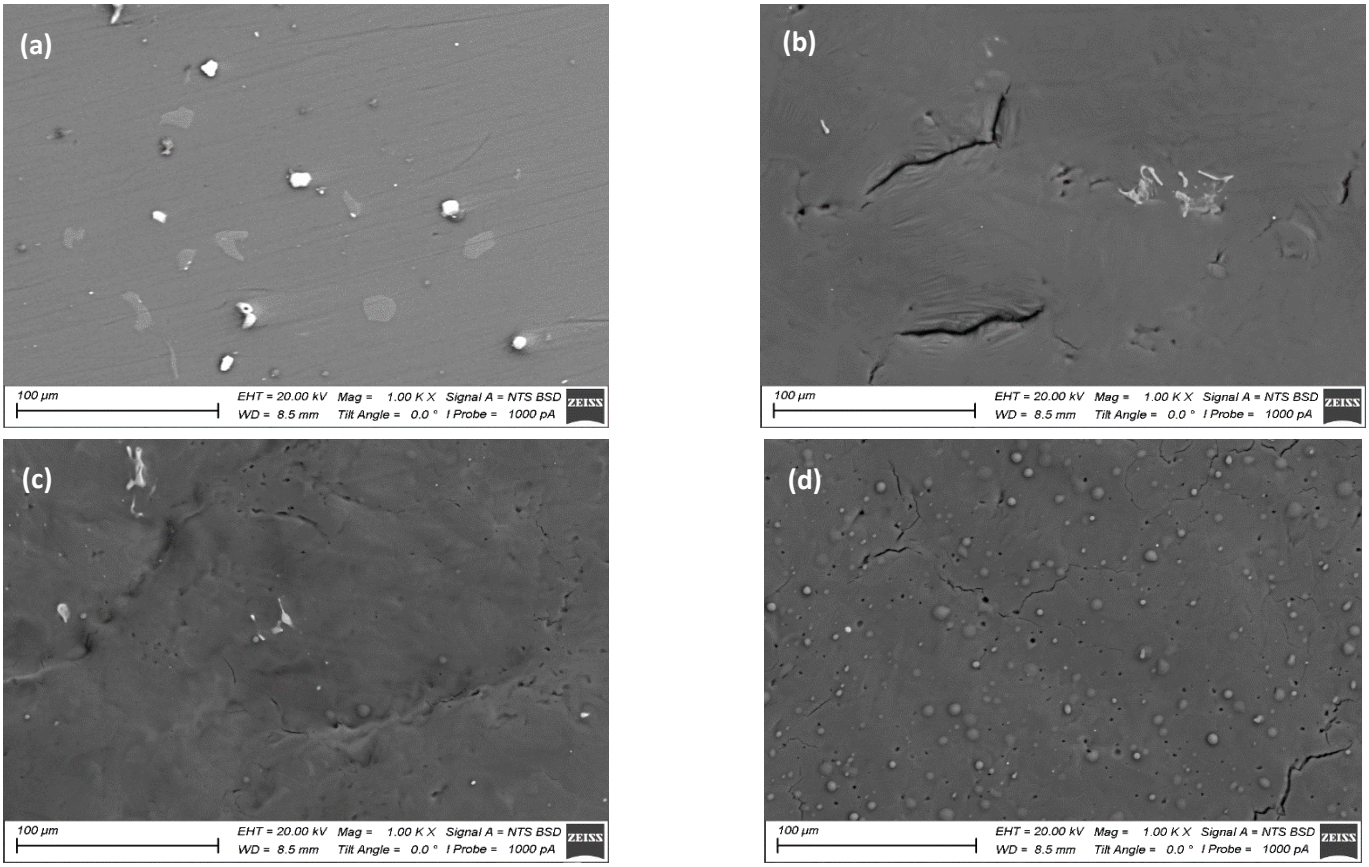

Fig. 10. SEM images of samples for the surface with 1000X magnification, including (a) the as-received material and surface-modified specimen under the surface energy of (b) 3, (c) 5, and (d) 8 J/cm^2

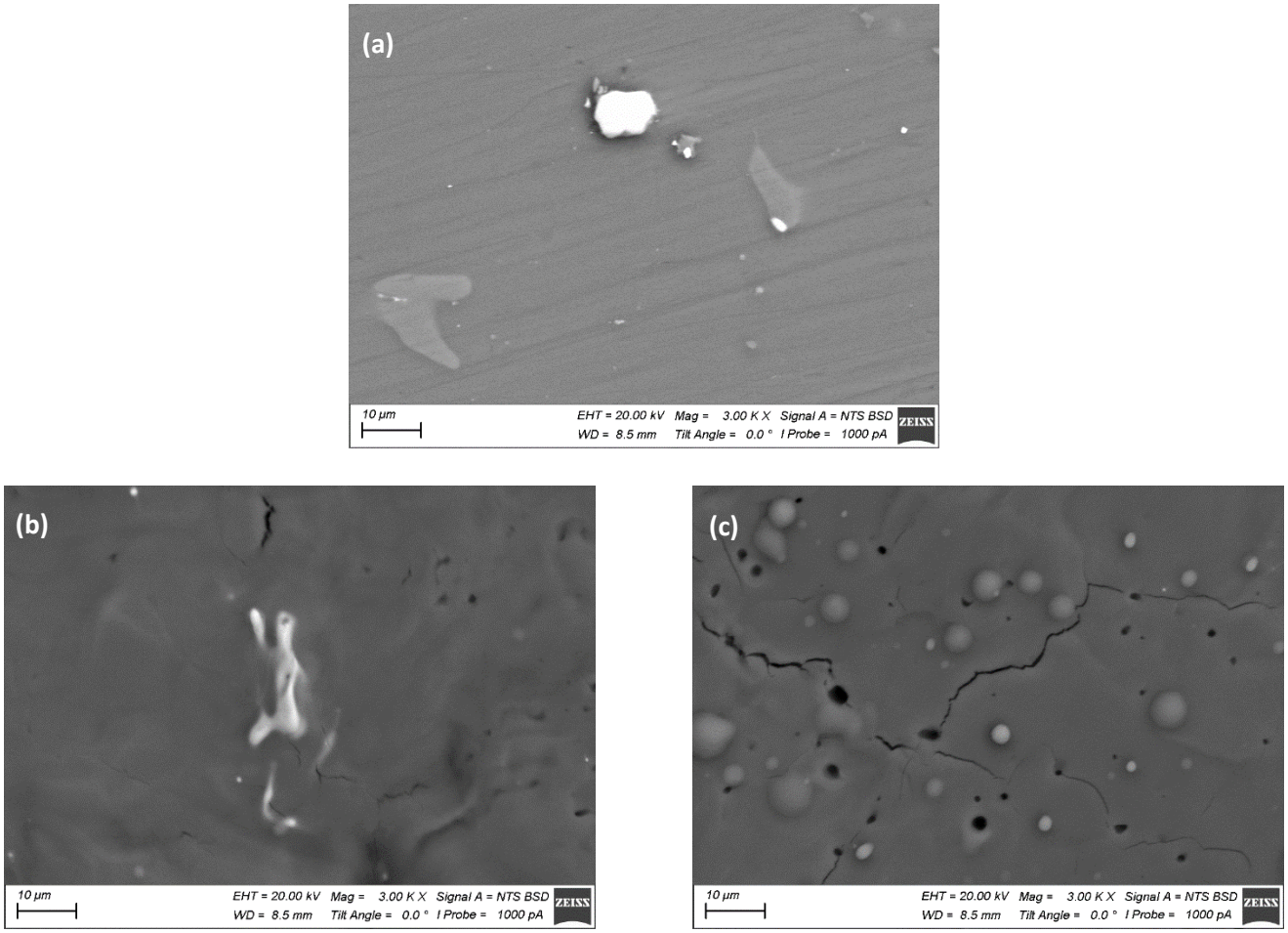

Fig. 11. SEM images of samples for the surface with 3000X magnification, including (a) the as-received material and surface-modified specimen under the surface energy of (b) 5 and (c) 8 J/cm^2

Table 6
The number and the averaged length of cracks

SEM magnification	Crack characteristics	Without modification	PEBI surface energy		
			3 J/cm^2	5 J/cm^2	8 J/cm^2
1000X	Number of cracks	1	3	35	43
250X	Number of cracks	1	45	10	59
1000X	Crack length (µm)	5.0±0.0	63.4±73.1	8.9±4.3	19.6±12.0
250X	Crack length (µm)	9.2±0.0	41.0±19.5	24.5±9.2	79.1±43.6

According to Table 6, it was found that among the three levels of 3, 5, and 8 J/cm^2, the value of 5 J/cm^2 had the least number of cracks and the shortest crack length.

Table 7 is depicted for showing the area of the phases, which were measured by the ImageJ software, from Figures 9 to 11. The PEBI process, in general, caused the percentage of the AlMn phase to be lower than the raw sample, and even at the energy level of 8 j/cm^2, the AlMn phase could be ignored. However, the percentage of $Mg_{17}Al_{12}$ phase after the PEBI process increased significantly.

4. Discussion

In the as-cast condition, the SEM microstructure of the AM60 alloy has various quantities of Ca [22]. As it could be observed in the literature [22], the alloy had a dendritic microstructure and also second-phase particles, which were distributed in the interdendritic regimes. Based on the SEM image, the alloy had bulky $Mg_{17}Al_{12}$ particles and discontinuous precipitations [22]. The majority of the β-$Mg_{17}Al_{12}$ intermetallic particles, detected in interdendritic zones were bulky particles, which had irregular morphology. Then also, the rest of the material was found as discontinuous β-$Mg_{17}Al_{12}$ precipitates [22].

Based on the literature [23-24], images were taken from the surface of AZ31 specimens using 15 kV and 22.5 kV for the accelerating voltages in the large pulse electron beam (LPEB) technique, with the hue and brightness changing as the number of cycles increased (1, 10, 20, 40, and 100 cycles). The accelerating voltage of 15 kV and the surface energy of 3 J/cm^2 were considered by Hao and Li [18], Bo et al. [17], and Gao et al. [23], for the surface treatment of magnesium alloys with a high-current pulsed electron beam (HCPEB). Despite the fact that the tool mark on the bare surface was eliminated in all specimens, 1 and 10 cycle surfaces were poorer than the initial state.

Nonetheless, it had a brighter surface after 20 and 40 cycles. However, at 100 cycles, the little part's color went to black. As a result, when the LPEB process was used with an insufficient number of cycles, the surface of magnesium alloys could not be entirely converted to a new surface layer, and vice versa. In addition, edge deformation was seen in 22.5 kV samples. Some cracks were found at the edge, especially in the 100 cycle case. The crack was thought to be a major mechanical flaw generated by tensile stress caused by increased brittleness.

Lee [24] indicated that the surface of both AM60 and AZ91 specimens when the accelerating voltage increased from 15 to 30 kV and the cycle number increased to 40. Moreover, the surface was not brilliant at 15 kV, but it was bright at 22.5 and 30 kV. Moreover, despite having varying Al concentrations, the difference between AM60 and AZ91 was not significant, up to 22.5 kV. However, it appeared that the β-precipitation might be generated on the AZ91 surface when the accelerating voltage was set to 30 kV. Furthermore, due to numerous craters, the surface roughness of 30 kV appeared to be slightly high for use in engineering applications. It was thought that the energy density parameter was used to indicate the LPEB accelerating voltage, which was equal to 3, 5, 7, and 10 J/cm^2 [24].

The energy density parameter in AM60 produces comparable results. Small particles were identified in the AM60 surface's enlarged pictures. Higher energy density circumstances caused the particles to grow in size. The aggregated mountain of particles appeared evenly at 10 J/cm^2. The alloying effects are thought to have caused the active formation of β-$Mg_{17}Al_{12}$ particles in the treated surface by LPEB at high energy density conditions [24]. The identity of the particles, which were aggregated in the treated AM60 surface by LPEB could be verified [24]. The particle's Al concentration was unusually high compared to other regions. As a result, the remaining $Mg_{17}Al_{12}$ components were assumed to have aggregated and not consolidated in the Mg grains.

Table 7
The calculation of the phase area with SEM pictures by magnitude 250X and 1000X

Condition	Phase	Area
As-received (250X)	AlMn	0.32%
	$Mg_{17}Al_{12}$	1.08%
	MgO	0.12%
As-received (1000X)	AlMn	0.54%
	$Mg_{17}Al_{12}$	1.80%
	MgO	0.26%
PEBI by 3 j/cm^2 (250X)	AlMn	0.29%
	$Mg_{17}Al_{12}$	6.40%
PEBI by 3 j/cm^2 (1000X)	AlMn	0.43%
	$Mg_{17}Al_{12}$	16.3%
PEBI by 5 j/cm^2 (250X)	AlMn	0.06%
	$Mg_{17}Al_{12}$	20.80%
PEBI by 5 j/cm^2 (1000X)	AlMn	0.34%
	$Mg_{17}Al_{12}$	21.20%
PEBI by 8 j/cm^2 (250X)	AlMn	0.05%
	$Mg_{17}Al_{12}$	21.40%
PEBI by 8 j/cm^2 (1000X)	AlMn	0.01%
	$Mg_{17}Al_{12}$	22.80%

5. Conclusions

In this study, The effects of three levels of energy density (3, 5, and 8 j/cm^2) in pulsed electron beam irradiation (PEBI) technique on surface characteristics of AM60 magnesium alloy have been investigated. The following results were obtained.

- besides the Mg element, the intermetallic phases of Al-Mn and Mg-Al ($Mg_{17}Al_{12}$) were observed on the microstructure of all samples.
- Due to oxidation, the MgO phase was removed by the PEBI process which was observed in the as-received samples. The MgO phase amount in the AM60 alloy was very low. In general PEBI process caused the percentage of the AlMn phase to be lower than the raw samples, and even at the energy level of 8 j/cm^2, the AlMn phase could be ignored. However, the percentage of the $Mg^{17}Al^{12}$ phase increased significantly after the PEBI process and this phase changed from block to point mode and spread throughout the material.
- It was found that the PEBI process changed the surface characteristic and among the three levels of energy density, 5 J/cm^2 had the least number of cracks and the shortest crack length.

Acknowledgment

This work has been supported by the Center for International Scientific Studies & Collaboration (CISSC), Ministry of Science, Research and Technology in Iran. A part of this work (PEBI, SEM, and XRD) was performed according to the Russian Government research assignment for ISPMS SB RAS, project FWRW-2021-0003. Access to the experimental equipment in the “Nanotech” Common Use Center (ISPMS-SB-RAS) is acknowledged.

References

[1] I.J. Polmear, Magnesium alloys and applications, Mater. Sci. Technol. 10 (1994) 1–16.
[2] S. Shrestha, Magnesium and surface engineering, Surf. Eng. 26 (2010) 313–316.
[3] M. Azadi, G.H. Farrahi, G. Winter, W. Eichlseder, Fatigue lifetime of AZ91 magnesium alloy subjected to cyclic thermal and mechanical loadings, Mater. Des. 53 (2014) 639–644.
[4] M. Mokhtarishirazabad, M. Azadi, G.H. Farrahi, G. Winter, W. Eichlseder, Improvement of high temperature fatigue lifetime in AZ91 magnesium alloy by heat treatment, Mater. Sci. Eng. A 588 (2013) 357–365.
[5] M. Mokhtarishirazabad, S.M.A. Boutorabi, M. Azadi, M. Nikravan, An investigation of high cycle fatigue behavior of magnesium alloy for cylinder head application, J. Engine Res. 24 (2011) 29–35.

[6] D. Lee, B. Kim, S.M. Baek, J. Kim, H.W. Park, J.G. Lee, S.S. Park, Microstructure and corrosion resistance of a Mg_2Sn-dispersed Mg alloy subjected to pulsed electron beam treatment, J. Magnes. Alloy. 8 (2020) 345–351.

[7] D.I. Proskurovsky, V.P. Rotshtein, G.E. Ozur, A.B. Markov, D.S. Nazarov, V.A. Shulov, Y.F. Ivanov, R.G. Buchheit, Pulsed electron-beam technology for surface modification of metallic materials, J. Vac. Sci. Technol. A Vacuum, Surfaces, Film. 16 (1998) 2480–2488.

[8] B. Gao, S. Hao, J. Zou, W. Wu, G. Tu, C. Dong, Effect of high current pulsed electron beam treatment on surface microstructure and wear and corrosion resistance of an AZ91HP magnesium alloy, Surf. Coatings Technol. 201 (2007) 6297–6303.

[9] S. Hao, X. Zhang, X. Mei, T. Grosdidier, C. Dong, Surface treatment of DZ4 directionally solidified nickel-based superalloy by high current pulsed electron beam, Mater. Lett. 62 (2008) 414–417.

[10] J. Kim, S.S. Park, H.W. Park, Corrosion inhibition and surface hardening of KP1 and KP4 mold steels using pulsed electron beam treatment, Corros. Sci. 89 (2014) 179–188.

[11] Y. Samih, G. Marcos, N. Stein, N. Allain, E. Fleury, C. Dong, T. Grosdidier, Microstructure modifications and associated hardness and corrosion improvements in the AISI 420 martensitic stainless steel treated by high current pulsed electron beam (HCPEB), Surf. Coatings Technol. 259 (2014) 737–745.

[12] J. Kim, H.W. Park, Influence of a large pulsed electron beam (LPEB) on the corrosion resistance of Ti-6Al-7Nb alloys, Corros. Sci. 90 (2015) 153–160.

[13] Y.R. Liu, K.M. Zhang, J.X. Zou, D.K. Liu, T.C. Zhang, Effect of the high current pulsed electron beam treatment on the surface microstructure and corrosion resistance of a Mg-4Sm alloy, J. Alloys Compd. 741 (2018) 65–75.

[14] Z. Zhang, J. Cai, L. Ji, X. Wang, Y. Li, S. Yang, P. Lv, X. Hou, Q. Guan, Microstructures and corrosion mechanism of AISI 304L stainless steel irradiated by high current pulsed electron beam, Prot. Met. Phys. Chem. Surfaces. 50 (2014) 650–658.

[15] V.P. Rotshtein, V.A. Shulov, Surface modification and alloying of aluminum and titanium alloys with low-energy, high-current electron beams, J. Metall. 2011 (2011) 673685.

[16] J.C. Walker, J.W. Murray, M. Nie, R.B. Cook, A.T. Clare, The effect of large-area pulsed electron beam melting on the corrosion and microstructure of a Ti6Al4V alloy, Appl. Surf. Sci. 311 (2014) 534–540.

[17] G. Bo, H. Yi, Z. Wenfeng, T. Ganfeng, Surface modification of Mg alloys AZ31 and ZK60-1Y by high current pulsed electron beam, Spec. Issues Magnes. Alloy., IntechOpen Publication (2011).

[18] S. Hao, M. Li, Producing nano-grained and Al-enriched surface microstructure on AZ91 magnesium alloy by high current pulsed electron beam treatment, Nucl. Instruments Methods Phys. Res. Sect. B Beam Interact. with Mater. Atoms. 375 (2016) 1–4.

[19] X.D. Zhang, S.Z. Hao, X.N. Li, C. Dong, T. Grosdidier, Surface modification of pure titanium by pulsed electron beam, Appl. Surf. Sci. 257 (2011) 5899–5902.

[20] M.E. Ikpi, J. Dong, W. Ke, Electrochemical investigation of the galvanic corrosion of AM60 and AD62 magnesium alloy in 0.1 M NaCl solution, Int. J. Electrochem. Sci. 10 (2015) 552–563.

[21] A. Kula, T. Tokarski, M. Niewczas, Comparative studies on the structure and properties of rapidly solidified and conventionally cast AM60 magnesium alloys, Mater. Sci. Eng. A 759 (2019) 346–356.

[22] B. Kondori, R. Mahmudi, Effect of Ca additions on the microstructure, thermal stability and mechanical properties of a cast AM60 magnesium alloy, Mater. Sci. Eng. A. 527 (2010) 2014–2021.

[23] B. Gao, S. Hao, J. Zou, T. Grosdidier, L. Jiang, J. Zhou, C. Dong, High current pulsed electron beam treatment of AZ31 Mg alloy, J. Vac. Sci. Technol. A Vacuum, Surfaces, Film. 23 (2005) 1548–1553.

[24] W.J. Lee, Fabrication and characterization of corrosion-resistant surface layer on Mg-alloys by using large- pulsed electron beam (LPEB) irradiation process, MSc Thesis, Department of Mechanical Engineering, Ulsan National Institute of Science and Technology (2017).